Journal of Solid State Chemistry **144,** 188–194 (1999)
Article ID jssc.1999.8146, available online at http://www.idealibrary.com on IDEAL®

Calorimetric Investigation of Tricritical Behavior in Tetragonal $Pb(Zr_xTi_{1-x})O_3$

George A. Rossetti, Jr.[1]

Center for Advanced Microgravity Materials Processing, Department of Chemical Engineering, Northeastern University, Boston, Massachusetts 02115
E-mail: grossett@coe.neu.edu

and

Alexandra Navrotsky

Thermochemistry Facility, Chemistry Building, Department of Chemical Engineering and Materials Science, University of California, Davis, California 95616

Received September 3, 1998; accepted December 20, 1998

The order of the cubic ↔ tetragonal phase change in ferroelectric $Pb(Zr_xTi_{1-x})O_3$ (PZT) was investigated by measurements of the specific heat. The specimens studied were highly crystalline powder samples carefully prepared by chemical synthesis methods to ensure chemical homogeneity. The existence of a tricritical point in the compositional range $0.30 \leq x \leq 0.40$ was established. The results demonstrated a close correspondence between the effects of hydrostatic pressure and the effects of zirconium substitution on the order of the transition. A relationship between the first-order character of the transition and the ionic packing density in the cubic structure was proposed. © 1999 Academic Press

Key Words: **PZT; ferroelectrics; phase transitions; perovskites; specific heat.**

1. INTRODUCTION

Tricritical behavior has been observed in a number of ferroelectric materials (1). At a tricritical point, the character of the paraelectric ↔ ferroelectric transition lies at the borderline between that of a first-order (discontinuous) and a second-order (continuous) phase change. For the ferroelectric perovskites, it has been shown that the order of the transition can be changed by the application of a hydrostatic pressure (2) or by a variation in chemical composition through ion substitution (3, 4).

Perovskite-structured ferroelectrics in the $Pb(Zr_xTi_{1-x})O_3$ (PZT) system provide an unusual example of a complete solid solution in which two tricritical points have been reported (5, 6). The tricritical behavior in the PZT system is of special interest because the compositional variation of the transition order provides a means to systematically investigate the underlying crystal chemistry and physics. Moreover, the probability of creating a domain wall below the Curie temperature is much greater for a second-order transition than for a tricritical transition (1), and the corresponding change in domain wall population has implications for the elastodielectric properties (7). Also, because the topology of the ferroelectric free-energy surface is determined by the order of the transition, a close relationship between the location of the tricritical points and the phase boundaries of the subsolidus temperature-composition diagram is expected (4, 8).

Unfortunately, several obstacles are encountered in experimental studies of tricritical phenomena in the PZT system. It is difficult to continuously vary the relevant thermodynamic parameters with the accuracy needed to arrive precisely at the tricritical points (9). Microcrystalline features of the sample, such as chemical heterogeneity and/or lattice imperfections, may also depend on composition, and can exert a considerable influence on the nature of the transition (10). Perhaps for these reasons, there are significant discrepancies in the reported compositions at which the tricritical points occur. The location of one tricritical point on the rhombohedral ($PbZrO_3$-rich) side of the phase diagram has been variously reported as $x = 0.94$ (9, 11), $x = 0.90$ (5), and $x = 0.78$ (6). Similarly, a second tricritical point on the tetragonal ($PbTiO_3$-rich) side of the phase diagram has been reported as $x = 0.28$ (5) and $x = 0.45$ (6). To the best of the authors' knowledge, no physical basis for the location of these tricritical points has yet been proposed.

To better define the tricritical behavior in the PZT system, an investigation of the specific heat should prove particularly advantageous. The specific heat (C_P) integrates over all possible temperature-dependent contributions to the free energy occurring on the time scale of the measurements.

[1] To whom correspondence should be addressed.

0022-4596/99 $30.00

These contributions include the thermal evolution of the primary order parameter as well as contributions arising from coupling with other possible relaxations of the structure. The specific heat is also very sensitive to the presence of lattice defects that influence the phase transition but may not be clearly revealed in X-ray diffraction or dielectric permittivity measurements.

In the present communication, we report the results of differential scanning calorimetry experiments carried out on the cubic ↔ tetragonal phase transition in $Pb(Zr_xTi_{1-x})O_3$. The specimens studied were well-crystallized powder samples carefully prepared by chemical synthesis methods. The reduction in the first-order character of the transition with increasing zirconium substitution was studied. The results confirmed the existence of a tricritical point and suggested a relationship between the ionic packing density in the cubic phase and the order of the phase transition.

2. EXPERIMENTAL

The $PbTiO_3$ specimen was prepared from lead acetate trihydrate and titanium isopropoxide according to a solution–gelation procedure. The synthesis, structural characteristics, and thermodynamic properties of this specimen have been previously studied in detail are reported elsewhere (12, 13). The $Pb(Zr_xTi_{1-x})O_3$ materials ($x = 0.15$, 0.30, 0.40) were prepared by a metal–organic decomposition process using lead acetate trihydrate, zirconium acetate, and titanium acetylacetonate (14). The starting chemicals were assayed both by gravimetry and inductively coupled plasma spectroscopy. The required quantities of each reagent were measured by weight, dissolved in methanol (4–7 g/g titanium reagent), and gently evaporated to dryness. The metal-organic precursors so obtained were powdered in an agate mortar and pestle and transferred to platinum crucibles for decomposition in air at 1023 K. The resulting metal oxides were pelletized, sealed in platinum capsules to inhibit volatilization of PbO, and calcined to a higher temperature of 1323 K to increase phase purity and crystallinity.

High-resolution X-ray powder diffraction data were collected on a Siemens D500 diffractometer equipped with a focusing Ge crystal incident beam monochromator and a scanning linear position sensitive detector. The specimens were uniformly deposited onto a zero-background rotating specimen stage and data were collected in wide-angle scans (18°–98° 2θ) using Cu$K\alpha_1$ radiation. Precise lattice parameters were determined by the least-squares refinement method from 31 reflections appearing in the scan range using a LaB_6 external reference standard (15). The X-ray data showed that all of the samples were extremely well crystallized, exhibiting sharp diffraction profiles to high angles. Careful inspection of the background revealed no anomalous scattering and no reflections associated with secondary phases. Because the a lattice parameter of tetragonal PZT is strongly composition dependent (see Table 1), the breadth of the 200 reflection provided a convenient measure of any macroscopic variations in composition (16). The 200 peak showed no exaggerated broadening, and in all cases, the full width at half-maximum was in the range of 0.071° to 0.10° 2θ. This compared to the instrumental broadening at this angle of 0.064° 2θ.

The chemical characteristics of the samples were further examined using a CAMECA SX50 electron microprobe. High spectral resolution X-ray measurements were performed using wavelength dispersive spectroscopy. The X-ray lines and standard materials used to calibrate for quantitative analyses were O$K\alpha$ (Al_2O_3), Pb$M\alpha$ (Pb), Ti$K\alpha$ ($SrTiO_3$), and Zr$L\alpha$ (ZrO_2). The primary electron beam was accelerated at 15 kV with a regulated beam current of 20 nA. Under these conditions, the excitation volume for point analysis was approximately 800 nm^3. Multipoint analyses conducted at 50 random locations on the sample with $x = 0.30$ gave values for $Pb/(Ti + Zr) = 1.012$ and $Zr/(Ti + Zr) = 0.302$, in excellent agreement with the intended stoichiometric ratios. The small, uniform standard deviations in the atomic percentages for all elements ($\sim 0.2\%$) also indicated good chemical homogeneity in the samples. Qualitative wavelength analysis revealed traces of Sn and Hf as the only detectable impurities. These impurities were undoubtedly introduced with the starting Pb and Zr chemicals.

The heat capacity measurements were made using a Netzsch 404 high-temperature differential scanning calorimeter. The calorimeter calibration was performed using data collected on a high purity α-alumina powder sample ($> 99.99\%$) that was calcined at 1773 K prior to the experiments to ensure phase purity, coarse crystallinity, and dryness. The sensitivity polynomial for the calorimeter was determined as the ratio of these data to the reference data

TABLE 1
Thermodynamic and Structural Parameters of $Pb(Zr_xTi_{1-x})O_3$

Parameter	$x = 0.00$	$x = 0.15$	$x = 0.30$	$x = 0.40$
T_c(K)[a]	765.5	741.5	713.4	691.7
$T_t^{heating}$(K)	764.2	745.3	714.5	685.8
$T_t^{cooling}$(K)	752.1	737.0	709.5	685.2
ΔT_t(K)	12.1	8.3	5.0	0.6
L (kJ/mol)	1.93	0.962	0.390	—
a (nm)	0.3899	0.3938	0.3976	0.4002
c (nm)	0.4153	0.4150	0.4149	0.4150
V_{UC} (nm^3)	0.06414	0.06436	0.06559	0.06645
$(c/a) - 1$	0.0651	0.0539	0.0435	0.0370
$[(c/a) - 1]^{1/2}$	0.255	0.232	0.209	0.192
t (numeral)	1.0207	1.0118	1.0030	0.9972

[a] From phase diagram (Ref. 18).

for a synthetic sapphire sample (17). The temperature calibration was provided by the manufacturer and was determined from the known melting points of several pure metals spanning the temperature range of operation.

The samples were tightly packed in covered, cylindrical platinum crucibles. After equilibrating the samples at 313 K, the specific heat measurements were made over the range 313 to 1073 K using a scan rate of 20 K/min. Data were collected in heating runs and were acquired in 2 K intervals under dry argon flowing at 15 mL/min. To obtain additional data closer to the transition, measurements were made both on heating and cooling using a smaller data acquisition interval of 0.5 K. The heat capacities (C_P) of the samples were determined by subtracting the data for the empty crucibles from the data for the crucibles plus samples. The transition temperatures (T_t) were determined by locating the extrema in the first derivatives of the $C_P(T)$ curves.

The order of the transition for each sample was characterized by the excess entropy (S^{xs}), the latent heat of transition (L), and the hysteresis in transition temperature ($\Delta T_t = T_t^{heating} - T_t^{cooling}$). To compute the quantities S^{XS} and L, the excess specific heat ($\Delta C_P = C_P - C_P^0$) was first determined from the heating curves by subtracting the background specific heat (C_P^0) from the raw $C_P(T)$ data. The background specific heat (i.e., the contributions to C_P not associated with the phase transition) was obtained as an extrapolation of the data for the cubic phase (C_P^{cubic}) into the transition region. Using the ΔC_P data, the excess entropy and latent heat were then determined from the following relations:

$$S^{xs} = \int \frac{\Delta C_P}{T} dT \text{ (excess entropy)}, \qquad [1]$$

$$L = \int_{T_P - \delta}^{T_P + \delta} \Delta C_P \, dT \text{ (latent heat)}, \qquad [2]$$

with $T_P = T$ at ΔC_P^{max} and $4.5 \leq \delta \leq 7.5$ K.

3. RESULTS AND DISCUSSION

The results of the specific heat measurements (313 to 1073 K) are shown in Fig. 1. The temperature dependence of C_P could be divided into four distinct regimes. At low temperatures, well below the transition point, the specific heat for all samples was nearly identical, rising from 109 J/[mol-K] at 323 K to 118 J/[mol-K] at 400 K. At these temperatures, the effect of the phase transition on C_P should be small and the measured values will reflect primarily the lattice (hard mode) contributions. At temperatures above 400 K, the C_P for the various samples began to differ and to increase markedly as the transition temperature for each was approached. Close to the transition temperature, all samples showed well-defined anomalies in C_P with no evidence of "smearing" that could be attributed to local fluctuations in composition or to other imperfections. Although the transition for each sample was sharp, there was a dramatic decrease in the peak value of C_P with increasing x. At

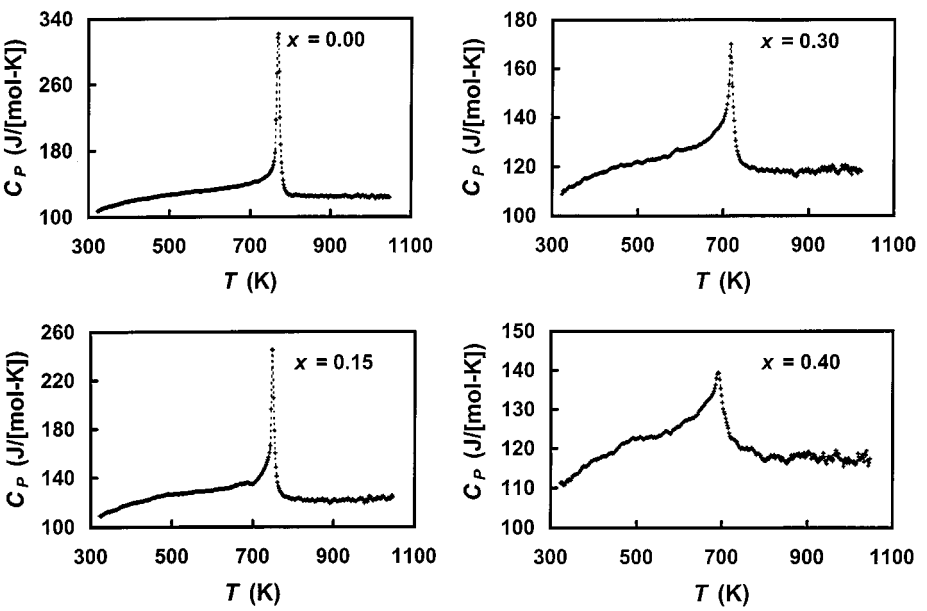

FIG. 1. Specific heat *versus* temperature for various compositions of tetragonal $Pb(Zr_xTi_{1-x})O_3$. Note that the ordinates of the plots have been adjusted to reflect the reduction in the maximum of C_P with increasing zirconium substitution (x).

temperatures above the transition point, the C_P for each sample dropped abruptly to a constant but composition-dependent value to temperatures as high as 1073 K.

The behavior of the specific heat obtained both on heating and cooling is compared for the various samples in Figs. 2 and 3. The change in the nature of the phase transition with increasing x was especially obvious in the measurements made on cooling. For the sample with $x = 0.00$, the C_P increased abruptly at the transition point, with virtually no premonitory rise as the transition temperature was approached. Similar behavior was observed for the sample with $x = 0.15$, while the increase for sample with $x = 0.30$ was appreciably more gradual. For these samples, there was clear evidence of a latent heat of transition. The values determined with an approximate uncertainty of ± 0.05 kJ/mol were $L = 1.93$, 0.96, and 0.39 kJ/mol for $x = 0.00$, 0.15, and 0.30, respectively. For the sample with $x = 0.40$, there was no detectable latent heat, with C_P at the transition showing only a step-like change characteristic of a second-order phase transition. Consistent with these observations, Fig. 4 shows that the hysteresis in transition

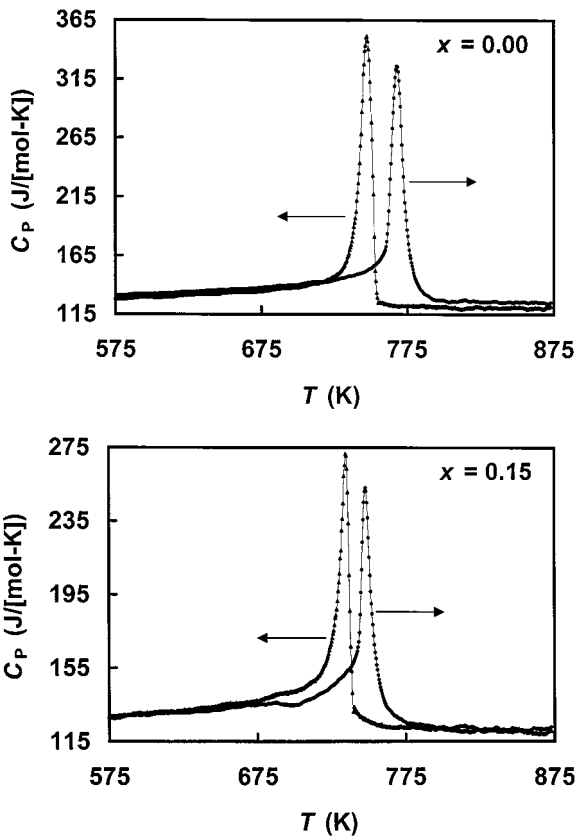

FIG. 2. Specific heat of tetragonal $Pb(Zr_xTi_{1-x})O_3$ as obtained on heating and cooling. Note that the ordinates of the plots have been adjusted to reflect the reduction in the maximum of C_P with increasing zirconium substitution (x).

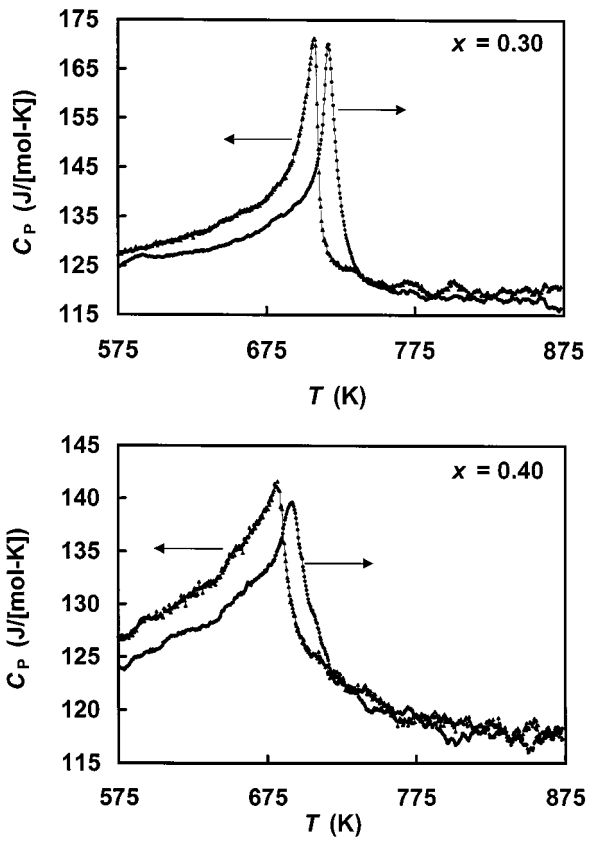

FIG. 3. Specific heat of tetragonal $Pb(Zr_xTi_{1-x})O_3$ as obtained on heating and cooling. Note that the ordinates of the plots have been adjusted to reflect the reduction in the maximum of C_P with increasing zirconium substitution (x).

temperature (ΔT_t) decreased with increasing x, from about 12 K for the sample with $x = 0.00$ to 5 K for the sample with $x = 0.30$. For the sample with $x = 0.40$, the hysteresis $\Delta T_t \leq 0.6$ K was at the limit of the resolution of the measurements. For all compositions, the measured transition temperatures were in good agreement with the accepted phase diagram (18).

The character of the phase transition for each sample is best characterized by the behavior of the excess entropy. To a good approximation, the Landau theory of phase transitions predicts that the excess entropy will vary as $S^{xs} = \alpha_0(x)P^2$, where $\alpha_0(x)$ is a composition-dependent constant and the spontaneous polarization P is the primary order parameter for the transition (19). As shown in Fig. 5, the behavior of S^{xs} (and hence P) near T_t was clearly discontinuous for the samples with $x = 0.00$ and $x = 0.15$, slightly discontinuous for $x = 0.30$, and continuous for the sample with $x = 0.40$. The combined data in Figs. 2–5 strongly suggest the existence of a tricritical point in the composition range $0.30 \leq x \leq 0.40$. High-resolution X-ray diffraction data (20) collected in 2 K intervals around the transition

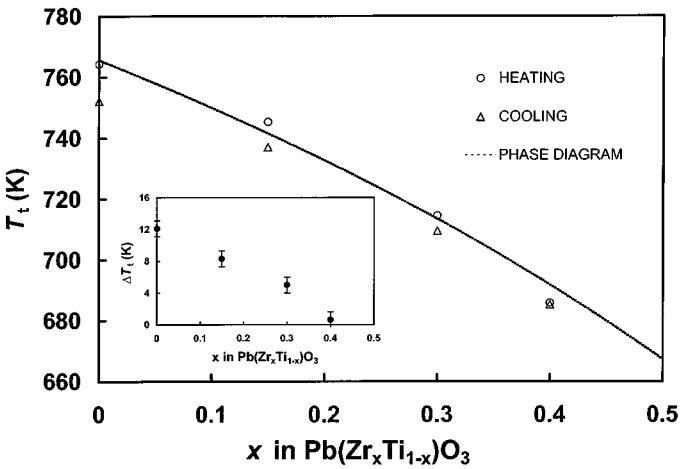

FIG. 4. Transition temperatures for tetragonal $Pb(Zr_xTi_{1-x})O_3$. The inset shows the rapidly vanishing thermal hysteresis for $x > 0.30$. The dashed line represents the expected Curie temperatures T_c based on the phase diagram given in Ref. 18.

points also confirmed this result. The X-ray data showed clear coexistence of the cubic and tetragonal phases for $x = 0.00$ and $x = 0.15$, a very narrow region of coexistence for the sample with $x = 0.30$, and no discernible coexistence for the sample with $x = 0.40$.

In understanding the observed reduction in the first-order character of the phase transition, it is instructive to compare the present results with those obtained under the application of hydrostatic pressure. For the perovskite ferroelectrics, the effect of hydrostatic stress on the order of the transition can be adequately explained by modifying the usual Landau–Devonshire form of the thermodynamic potential to include pressure dependencies of the elastic constants and/or the electrostrictive coupling coefficients (21).

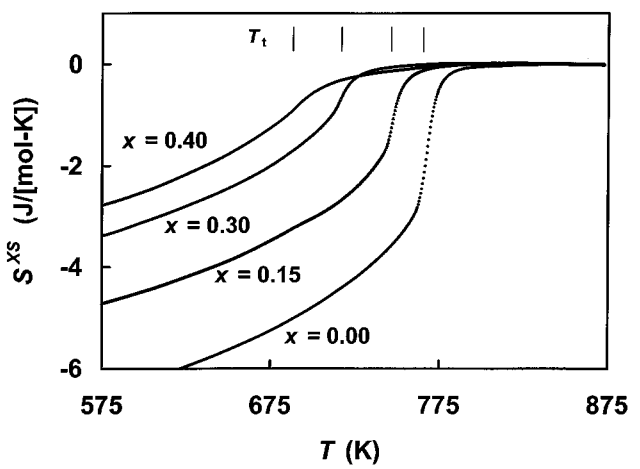

FIG. 5. Excess entropy *versus* temperature for various compositions of tetragonal $Pb(Zr_xTi_{1-x})O_3$.

In an analogous way, it has been proposed that ion substitutions influence the character of the transition by altering the elastic and/or electrostrictive properties at the microscopic level (9, 11).

Several investigators have studied the effect of hydrostatic pressure on the order of the phase transition in lead titanate (22, 23). X-ray measurements made at room temperature on single-crystal samples have revealed that the structure is much more compressible along the crystallographic *c*-axis than along the *a*-axis (24, 25). As shown in Fig. 6, at pressures (σ) less than the critical pressure (σ^*), the lattice parameter *c* decreased with pressure but the parameter *a* increased slightly. The net effect was that both the unit cell volume (V_{uc}) and the uniform spontaneous strain parameter ($z = c/a - 1$) decreased with increasing pressure. The uniform spontaneous strain varies with the primary order parameter as $z = qP^2$, where q is a constant related to the electrostrictive coupling coefficients. An analysis of these data (23) and of the corresponding room temperature plane of the T–σ–$z^{1/2}$ phase diagram has shown that a tricritical point occurs at $\sigma^* = 1.75$ GPa and $z^{1/2} = 0.195$. At a higher pressure of 11 GPa, the tetragonal structure undergoes a second-order transition to the cubic phase (26).

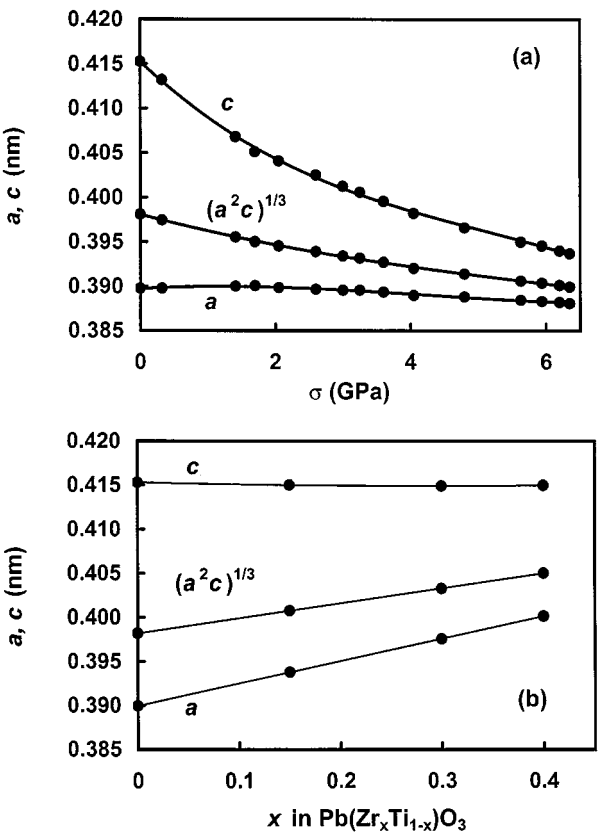

FIG. 6. Lattice parameters of $Pb(Zr_xTi_{1-x})O_3$. (a) Lattice parameters *versus* hydrostatic pressure for $PbTiO_3$ (from reference 24) and (b) Lattice parameters *versus* zirconium concentration in $Pb(Zr_xTi_{1-x})O_3$.

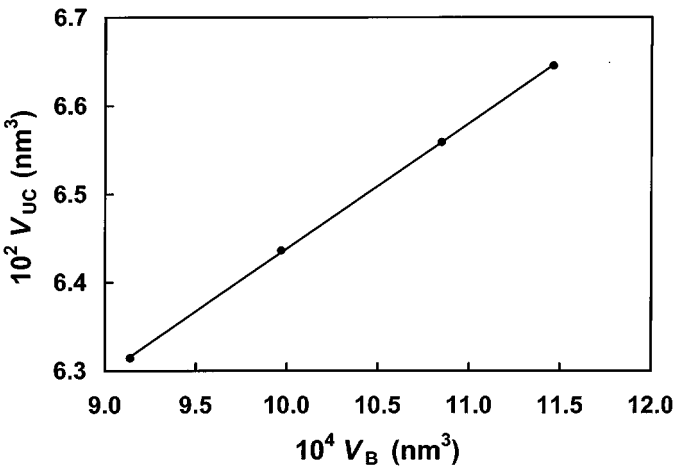

FIG. 7. Unit cell volume of tetragonal $Pb(Zr_xTi_{1-x})O_3$ *versus* B-site cation volume in the perovskite structure as computed from the ionic radii.

Qualitatively, the effect of zirconium substitution on several structural parameters of lead titanate is quite different. As seen in Table 1 and Fig. 6, the a lattice parameter increased with zirconium content while the c lattice parameter remained constant. The net effect was an *increase* in the unit cell volume. As shown in Fig. 7, this increase showed a nearly perfect correlation with the volume of the atoms (V_B) on the B-site of the ABO_3 perovskite structure as computed from the revised crystal radii (27).

However, as with the application of hydrostatic pressure, the uniform spontaneous strain decreased with increasing values of x. Assuming a direct correlation between the effects of pressure and composition on the order parameter P, the composition for which $z^{1/2}(x) = z^{1/2}(\sigma^*)$ was found to be $x^* = 0.38$. Figure 8 shows a plot of the square root of the uniform strain parameter ($z^{1/2} \propto P$) against the normalized pressure (σ/σ^*) and the normalized composition (x/x^*) on approaching the tricritical point ($\sigma/\sigma^* = x/x^* \to 1$). Both sets of data fall very closely on a single curve. This finding confirms that a close correspondence exists between the effect of hydrostatic pressure and the effect of zirconium substitution on the order of the transition.

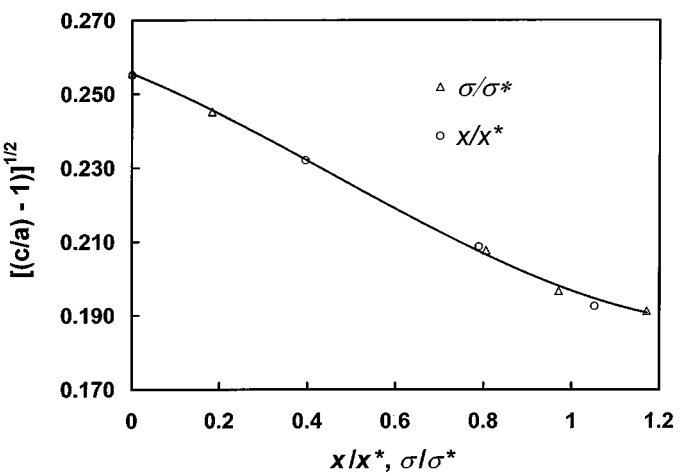

FIG. 8. Variation of the square root of the uniform deformation parameter *versus* normalized pressure for $PbTiO_3$ and normalized composition for $Pb(Zr_xTi_{1-x})O_3$ on approaching a tricritical point. Both sets of data fall on a single curve.

The relationship between the macroscopic effect of hydrostatic pressure and the microscopic effect of Zr substitution on the order of the transition most likely stems from the fact that both increase the degree of close-packing in the structure. For the ferroelectric perovskites, the degree of close-packing is usually represented by the tolerance factor (t), given by the equation

$$t = \frac{(r_A + r_X)}{\sqrt{2}(r_B + r_X)}, \qquad [3]$$

where r_A, r_B are the cation radii on the A and B lattice sites of the perovskite structure and r_X is the anion radius. For the ideally close-packed cubic structure, with all ions in contact, $t = 1$. However, real perovskite structures admit a considerable range of t, with the most likely interval being $0.707 \leq t \leq 1.225$. The deviation from the ideal close-packed structure leads to an instability in the ion positions, to increased oscillations at high temperatures, and, under appropriate thermodynamic conditions, to static ion displacements from the cubic structure to structures of lower symmetry, i.e., displacive phase transitions (28).

The tolerance factor for the various PZT samples studied are compared in Table 1, where it is shown that the value dropped linearly from $t = 1.0207$ for $x = 0.00$ to the value $t = 0.9972$ for $x = 0.40$. The composition for which the tolerance factor was unity was computed from the crystal radii to be $x = 0.35$. This composition is very close to the value $x^* = 0.38$, where, on the basis of the preceding discussion, the transition is expected to pass through a tricritical point at ambient pressure. Consequently, it appears that as the radius of the B-site cation is increased by Zr substitution, the tendency for displacement along the tetragonal $\langle 001 \rangle$ directions is decreased, and the character of the transition changes from first- to second-order. It should also be noted that at higher Zr concentrations ($x \approx 0.53$), the morphotropic phase boundary is approached, and the structure changes to rhombohedral symmetry with the polarization reorienting from the $\langle 001 \rangle$ to the $\langle 111 \rangle$ directions (18).

Some evidence for a change in the vibrational density of states (and hence the nature of the phase transition) can be inferred from the high-temperature heat capacity data. As mentioned previously, above the transition temperature, all samples showed a constant but composition-dependent heat capacity to temperatures as high as 1073 K. The

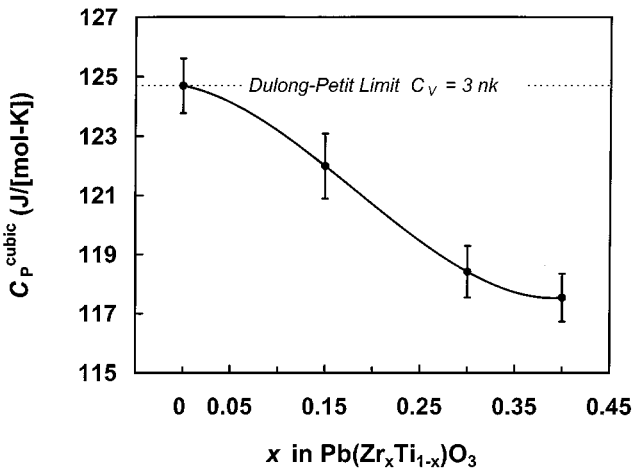

FIG. 9. Heat capacity of the cubic phase of $Pb(Zr_xTi_{1-x})O_3$ *versus* zirconium concentration. The dashed line represents the classical limit of Dulong and Petit for C_V.

specific heat of the cubic phase of lead titanate ($x = 0.00$) had an average value $C_P^{\text{cubic}} = 124.7 \pm 0.9$ J/[mol-K]. The Dulong and Petit limiting value for C_V is $3nk_b = 124.7$ J/[mol-K], and for solids at moderate temperatures, the difference $C_P - C_V = TV\alpha^2/\beta$ (where α is the thermal expansivity, β the compressibility) is typically less than 1% (29). Consequently, the excellent agreement of the measured C_P with the Dulong and Petit limit indicated that cubic lead titanate has an essentially constant heat capacity representative of full equipartition excitation of vibrational modes. In contrast, as shown in Fig. 9, the substitution of the larger Zr atom for Ti resulted in a marked decrease in C_P^{cubic} with increasing x. This decrease may be attributable to the higher degree of close-packing for these samples, which may alter the elastic or electrostrictive properties and lead to a change in the character of the cubic $\leftrightarrow$ tetragonal transition.

4. CONCLUSION

In summary, the order of the cubic $\leftrightarrow$ tetragonal phase change in highly crystalline powder samples of $Pb(Zr_xTi_{1-x})O_3$ was investigated by measurements of the specific heat. The existence of a tricritical point in the compositional range $0.30 \leq x \leq 0.40$ was established. The results demonstrated a close correspondence between the effects of hydrostatic pressure and the effects of zirconium substitution on the order of the transition and suggested a relationship between the character of the transition and the ionic packing density in the cubic structure. The location of the tricritical point was estimated to be in the vicinity of $x = 0.38$, close to the composition ($x = 0.35$) where the tolerance factor adopts a value of unity. The higher degree of close-packing near this composition may alter the elastic or electrostrictive properties of the lattice and lead to a change in the character of the phase transition.

ACKNOWLEDGMENTS

This work was initiated at Princeton University and was supported by the NSF Solid State Chemistry Program (Grants DMR 92-15802 and 97-03922) and used facilities of CHiPR, the Center for High Pressure Research, an NSF Science and Technology Center. Completion of this work was supported at the Center for Advanced Microgravity Materials Processing, a NASA sponsored Commercial Space Center. The authors are also indebted to Dr. J. P. Cline (National Institute of Standards and Technology) and Dr. E. Vicenzi (Princeton University) for their assistance with the X-ray diffraction and electron microprobe measurements.

REFERENCES

1. E. K. H. Salje, *Phase Transitions* **34,** 25 (1991).
2. R. Clarke and L. Benguigui, *J. Phys. C* **10,** 1963 (1977).
3. K. Bethe and F. Welz, *Mater. Res. Bull.* **6,** 209 (1971).
4. L. Benguigui and Y. Beaucamps, *Ferroelectrics* **25,** 633 (1980).
5. M. J. Haun, E. Furman, H. A. McKinstry, and L. E. Cross, *Ferroelectrics* **99,** 27 (1989).
6. V. V. Eremkin, V. G. Smotrakov, and E. G. Fesenko, *Ferroelectrics* **110,** 137 (1990).
7. C. A. Randall, G. A. Rossetti, Jr., and W. Cao, *Ferroelectrics* **150,** 163 (1993).
8. W. Cao and L. E. Cross, *Phys. Rev. B* **47,** 4825 (1993).
9. R. W. Whatmore, R. Clarke, and A. M. Glazer, *J. Phys. C* **11,** 3089 (1978).
10. K. S. Aleksandrov and I. N. Flerov, *Sov. Phys. Solid State* **21,** 195 (1979).
11. K. Roleder and J. Hańderek, *Phase Transitions*, **2,** 285 (1982).
12. G. A. Rossetti, Jr., L. E. Cross, and J. P. Cline, *J. Mater. Sci.* **30,** 24 (1995).
13. G. A. Rossetti, Jr., J. P. Cline, and A. Navrotsky, *J. Mater. Res.* **13,** 3197 (1998).
14. G. H. Haertling, "Proc. IEEE, 7th Int. Symp. on the Applications of Ferroelectrics" (S. B. Krupanidhi and S. K. Kurtz, Eds.), p. 292. IEEE, 1990.
15. S. D. Rasberry, Certificate of Analysis, SRM 660, National Institute of Standards and Technology, Gaithersburgh, MD (1989).
16. K. Kakegawa, K. Arai, Y. Sasaki, and T. Tomizawa, *J. Am. Ceram. Soc.* **71,** C-49 (1988).
17. D. A. Ditmars and T. B. Douglas, *J. Res. Natl. Bur. Stand.* **75A,** 401 (1971).
18. B. Jaffe, W. R. Cooke, Jr., and H. Jaffe, "Piezoelectric Ceramics," p. 136, Academic Press, New York, 1971.
19. E. K. H. Salje, "Phase Transitions in Ferroelastic and Co-elastic Crystals," Ch. 9, Cambridge University Press, Cambridge, 1990.
20. G. A. Rossetti, Jr., and J. P. Cline, unpublished.
21. L. Benguigui, *Phys. Stat. Sol.* (*b*) **60,** 835 (1973).
22. G. A. Samara, *Ferroelectrics* **2,** 277 (1971).
23. R. Ramírez, M. F. Lapeña, and J. A. Gonzalo, *Phys. Rev. B* **42,** 2604 (1990).
24. R. J. Nelmes and A. Katrusiak, *J. Phys. C* **19,** L725 (1986).
25. R. Ramírez, H. Vincent, R. J. Nelmes, and A. Katrusiak, *Solid State Commun.* **77,** 927 (1991).
26. C. S. Zha, A. G. Kalinichev, J. D. Bass, C. T. A. Suchicital, and D. A. Payne, *J. Appl. Phys.* **72,** 3705 (1992).
27. R. D. Shannon, *Acta Crystallogr. A* **32,** 751 (1976).
28. F. A. Kassan-Ogly and V. E. Naish, *Acta Crystallogr. B* **42,** 307 (1986).
29. A. Navrotsky, "Physics and Chemistry of Earth Materials," p. 280. Cambridge University Press, Cambridge, 1994.